Tuning the central wavelength by hundreds of nanometers using ultrafast molecular phase modulation

Zhiyuan Huang,[1,2] Ding Wang,[1] Yuxin Leng,[1,*] and Ye Dai[2,†]

[1]*State Key Laboratory of High Field Laser Physics, Shanghai Institute of Optics and Fine Mechanics, Chinese Academy of Sciences, Shanghai 201800, China*

[2]*Department of Physics, Shanghai University, Shanghai 200444, China*

(Received 6 February 2015; published 6 April 2015)

We theoretically study the central wavelength tuning of a laser pulse propagating in a hollow-core fiber filled with prealigned nitrogen gas. The simulation results show that the double pump pulses, suitable pump pulse energy, gas pressure, and temperature can extend the wavelength shift range, and the spectral blueshift or redshift can be controlled by tuning the time delay between the pump and probe pulses. It is also shown that several hundred nanometers wavelength tuning is obtained by the double pump pulses with appropriate parameters.

DOI: 10.1103/PhysRevA.91.043809 PACS number(s): 42.65.Jx, 42.65.Re, 33.80.−b

I. INTRODUCTION

Ultrashort femtosecond laser pulses have a wide variety of applications in science and technology such as high-order-harmonic generation [1], attosecond pulse generation [2,3], chemical reaction dynamics [4,5], and time-resolved measurements in atomic and molecular physics [6]. Femtosecond Ti:sapphire lasers based on the traditional chirped-pulse amplification (CPA) technique are now widely used sources of stable, energetic femtosecond pulses [7,8]. However, wavelength tuning directly from the laser system is limited to a narrow range around the fundamental wavelength of 800 nm. The central wavelength tuning range can be greatly improved by using optical parametric amplification (OPA) or the newly proposed optical parametric chirped-pulse amplification (OPCPA) [9–11], but the efficiency is restricted because it is difficult to satisfy phase matching precisely, and the systems are complicated. Spectral shifts could also be achieved by producing laser filaments in atom gases and by monitoring compression and self-steepening events by varying the pump wavelength, the pressure, and the nature of the gas undergoing photoionization [12–14]. An alternative mechanism for ultrashort pulse spectral conversion called molecular phase modulation (MPM) has also been demonstrated [15,16]. It is based on impulsive molecular alignment in Raman-active gases, where an ultrashort pulse first propagates through the molecular gas and excites impulsively molecular alignment; then a time-delayed probe pulse experiences a rapid phase modulation due to refractive index variation caused by the molecular alignment revivals [17–21]. With such methods [22], the central wavelength of an initial 800-nm, 5-fs Gaussian pulse is theoretically shown to be tuned from 324.6 to 4237.3 nm by using impulsively excited molecular alignment created by another 800-nm, 100-fs laser pulse of intensity 3.5×10^{13} W/cm^2, which is very promising as a tunable source. In order to gain more insight into the propagation dynamics involved for future implementation, a more accurate model is needed to include effects such as waveguide attenuation and dispersion, ionization, plasma defocusing, and so on.

In this work, we theoretically study the spectral modulation of an ultrashort laser pulse propagating in a hollow-core fiber (HCF) filled with prealigned nitrogen gas, which shows a blueshift or redshift by changing the time delay between the pump and the probe pulses. It is found that hundreds of nanometers wavelength tuning is obtained by ultrafast molecular phase modulation in prealigned nitrogen molecules.

II. THEORETICAL MODEL

A. Molecular alignment

When a linear molecule is subjected to the laser pulse field $E(t) = E_0 f(t)\cos(\omega_0 t)$, where E_0 is the amplitude, $f(t) = \exp[-(2\ln 2)t^2/\tau^2]$ is the Gaussian shape, τ is the pulse full width at half maximum (FWHM), and ω_0 is the central frequency of laser field, the evolution of the molecular state can be described based on a rigid-rotor model as [23]

$$i\hbar\partial_t|\psi(\theta,t)\rangle = H(t)|\psi(\theta,t)\rangle, \tag{1}$$

where $H(t)$ is the total interaction Hamiltonian and is given by [24]

$$H(t) = B\mathbf{J}^2 - \mu_0 E(t)\cos\theta - \tfrac{1}{2}[(\alpha_{//} - \alpha_\perp)\cos^2\theta + \alpha_\perp]E^2(t), \tag{2}$$

where B is the molecular rotational constant and $\mathbf{J}$ is the operator of the angular momentum (with the eigenvalue of non-negative integer and the reduced Planck constant $\hbar$ factor absorbed in constant B); μ_0 is the molecular permanent dipole moment, θ is the angle between the laser polarization and the molecular axis, and $\alpha_{//}$ and $\alpha_\perp$ are the polarizabilities in the direction parallel and perpendicular to the molecular axis. The first term on the right-hand side of Eq. (2) describes the molecular rotational energy; the other two terms represent the interaction potentials with the permanent dipole moment and the polarizability, respectively. Finally, the degree of the molecular alignment is characterized by the expectation value

*lengyuxin@siom.ac.cn
†yedai@shu.edu.cn

of $\cos^2\theta$. Considering the thermal equilibrium of the molecular ensemble, the alignment is averaged over the Boltzmann distribution and expressed as [25]

$$\begin{aligned}\langle\langle\cos^2\theta\rangle\rangle &= \sum_J W_J \sum_{M=-J}^{J} \langle\psi_{J,M}|\cos^2\theta|\psi_{J,M}\rangle \\ &= \sum_J \frac{g_J \exp[-BJ(J+1)/kT]}{Q} \\ &\quad\times \sum_{M=-J}^{J} \langle\psi_{J,M}|\cos^2\theta|\psi_{J,M}\rangle, \end{aligned} \tag{3}$$

where W_J is the Boltzmann weight factor; $\psi_{J,M}$ is the rotational wave function of the evolved molecules, the g_J factor reflects the nuclear spin statistics of the molecule, Q is the rotational partition function, k is the Boltzmann constant, and T is the molecular rotational temperature.

B. Molecular phase modulation based on HCF

In order to simulate the pulse propagation in HCF filled with molecular gases, the input electric field $E(r,t,z)$ is decomposed into a set of leaky modes, $E(r,t,z) = \sum_p U_p(t,z)\, V_p \exp[i\beta_p^{(0)} z - i\omega_0 t] + \text{c.c.}$, where p indicates the mode order EH_{1p}, $U_p,\{p = 1,2\cdots\}$ are the envelopes of different modes, $V_p = J_0(u_p r/a)$ is the zero-order Bessel function, u_p is the pth zero point of J_0, $\beta_p^{(0)}$ is the propagation constant at carrier frequency ω_0 of mode EH_{1p}, and a is the inner radius of HCF. The derivation of mode-coupling propagation equations is elaborated in [26], and given as follows for fundamental mode EH_{11}:

$$\begin{aligned}(\partial_z - iL_1)U_1 = {}& \frac{i\omega_0\hat{T}n_2}{c}\left[h_1|U_1|^2U_1 + \sum_{p\neq 1} h_p\left(U_1^2U_P^* e^{i\beta_1^{(0)}z - i\beta_p^{(0)}z} + 2|U_1|^2U_p e^{i\beta_p^{(0)}z - i\beta_1^{(0)}z}\right)\right] + \frac{i\omega_0\hat{T}}{c}\sum_p \delta n_p U_p e^{i\beta_p^{(0)}z - i\beta_1^{(0)}z} \\ & - \frac{\sigma}{2}\left[\sum_p d_p U_p e^{i\beta_p^{(0)}z - i\beta_1^{(0)}z}\right] - \frac{1}{2}\left[\frac{f_1}{U_1^*} - \sum_{p\neq 1}\frac{f_p}{(U_1^*)^2}U_p^* e^{i\beta_1^{(0)}z - i\beta_p^{(0)}z}\right] - \frac{iq_e^2}{2c\omega_0 m_e\varepsilon_0}\hat{T}^{-1}\left[\sum_p d_p U_p e^{i\beta_p^{(0)}z - i\beta_1^{(0)}z}\right], \end{aligned} \tag{4}$$

where the envelopes $U_p,\{p = 1,2\cdots\}$ are normalized to intensities. Linear operators $L_p = i\alpha_p^{(0)} - \alpha_p^{(1)}\partial_\tau + \sum_{m=2}^{\infty}(i\partial_\tau)^m[\beta_p^m + i\alpha_p^m]/m!$ describe the waveguide mode attenuation α and dispersion β with $\alpha_p^{(m)} = d^m\alpha_p/d\omega^m|_{\omega=\omega_0}$ and $\beta_p^{(m)} = d^m\beta_p/d\omega^m|_{\omega=\omega_0}$. The form of the linear operator is much simpler in the frequency domain which includes all orders of dispersion. The retard frame is moving at the group velocity of the fundamental mode $\tau = t - \beta_1^{(1)}z$. The constants c, σ, q_e, m_e, ε_0, and n_2 are light speed in vacuum, impact ionization cross section, electron charge and mass, vacuum permittivity, and instantaneous Kerr nonlinear refractive index, respectively. $\delta n_p = \int_0^a \Delta n V_1 V_p\, rdr/\int_0^a V_1^2\, rdr$ describes the effect of change of refractive index Δn induced by molecular rotation projected on the pth mode. The change of refractive index induced by molecular rotation can be calculated by either a simple "weak field" model or "strong field" model as $\Delta n(t,r,z) = 2\pi(\rho_0\Delta\alpha/n_0)[\langle\langle\cos^2\theta\rangle\rangle(t,r,z) - 1/3]$ where ρ_0 is the neutral density of gas; $\Delta\alpha$ is the polarizability difference between parallel to and perpendicular to the molecular axis [27,28]. The operator $\hat{T} = 1 + (i/\omega_0)\partial_\tau$ gives rise to self-steepening effects. The coefficients $h_p = \int_0^a V_1^3 V_p\, rdr/\int_0^a V_1^2\, rdr$, $d_p = \int_0^a \rho V_1 V_p\, rdr/\int_0^a V_1^2\, rdr$, and $f_p = \int_0^a \frac{V_p}{V_1}\eta W(\rho_0 - \rho)\, rdr/\int_0^a V_1^2\, rdr$ describe mode coupling involving instantaneous Kerr, plasma, and ionization effects. Assuming electrons born at rest, the electron density ρ evolves as

$$\frac{\partial\rho}{\partial t} = \eta W(I)(\rho_0 - \rho) + \frac{\sigma}{U_i}\rho I, \tag{5}$$

where the ionization rate $W(I)$ follows from the Perelomov-Popov-Terentiev (PPT) theory presented in [29], and U_i is the ionization potential. The coefficient $\eta = 1 + (1.5a_2 - 3.75a_4)(\langle\langle\cos^2\theta\rangle\rangle - 1/3) + 4.375a_4(\langle\langle\cos^4\theta\rangle\rangle - 1/5)$ describes the dependence of ionization rate on molecular alignment, where $a_2 = 0.39$ and $a_4 = -0.21$ [30].

In the following simulations, because the input pulse energy level is low, Eq. (4) can be further simplified by single-mode approximation as

$$\begin{aligned}(\partial_z - iL_1)U_1 = {}& \frac{i\omega_0\hat{T}n_2}{c}[h_1|U_1|^2U_1] + \frac{i\omega_0\hat{T}}{c}[\delta n_1 U_1] \\ & - \frac{\sigma}{2}d_1U_1 - \frac{1}{2}\left[\frac{f_1}{U_1^*}\right] - \frac{iq_e^2\hat{T}^{-1}}{2c\omega_0 m_e\varepsilon_0}[d_1U_1], \end{aligned} \tag{4'}$$

and for all input pulses (both pump and probe) the analytical form $U_1(t,z=0)$ at the input of the HCF is

$$U_1(t,z=0) = f_{\text{coup}}\sqrt{\frac{0.94E_{en}/\tau}{0.5\pi w_0^2}}\exp\left[-(2\ln 2)\frac{t^2}{\tau^2}\right], \tag{6}$$

where τ is the pulse FWHM, E_{en} is the pulse energy, w_0 is the $1/e^2$ radius of the beam intensity Gaussian profile at the focus just before the input of HCF, and f_{coup} is the fraction of the pulse that is coupled to the fundamental mode. The optimal coupling, i.e., where most of the energy is coupled to the fundamental mode, is met when $w_0 = 0.65a$, which corresponds to $f_{\text{coup}} \cong 0.88$.

It should be noted that in the modeling of pump-probe configurations, the propagation dynamics of both the pump pulses and the probe pulse are obtained by integration of Eq. (4). Since the electronic Kerr effect is instantaneous,

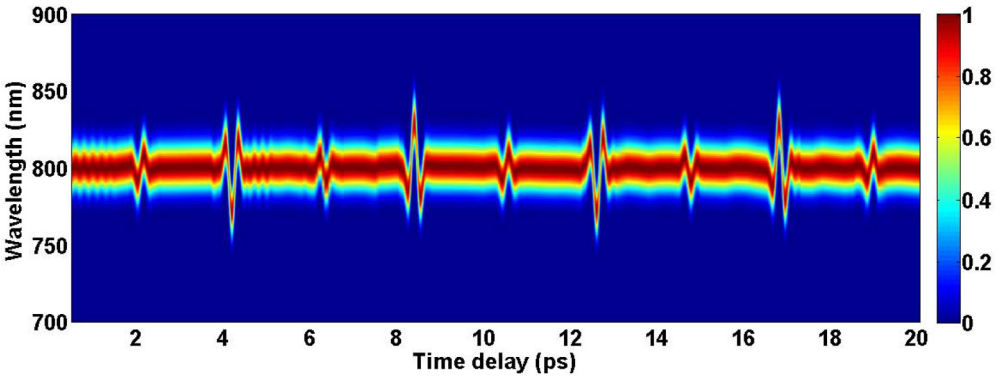

FIG. 1. (Color online) The spectral intensities of output probe pulse versus time delay between input pump and probe pulses with energy of 0.2 and 0.05 mJ, respectively. The gas pressure is set at 0.5 bar and the temperature is 25 °C.

this effect for different pulses is decoupled. However, as the lifetime of the molecular alignment and the plasma are of, or more than, picosecond level, and the delays between consecutive pulses are of picosecond level, these effects will be coupled between consecutive pulses. For the evaluation of molecular-rotation-induced Δn, the three-level model [28] is used for the first pulse. For the second pulse (the second pump or the probe), Δn is obtained by first integration of Eq. (1) with the first pulse and then free evolution of final states across the second pulse. For the third pulse, Δn is obtained by first integration of Eq. (1) with the first followed by the second pulses and then free evolution of final states across the third pulse. As for plasma generation, considering the lifetime is of nanosecond level, the recombination process is ignored and the initial electron density seen by a pulse is taken as that at the end of the former pulse (the initial electron density of the first pulse is taken as 0).

III. RESULTS AND ANALYSIS

In the simulation, we use the HCF filled with prealigned nitrogen gas with the length of 1 m and the inner diameter of 250 μm as an example, and the molecular parameters are $B/(hc) = 1.989581\,\mathrm{cm}^{-1}$ where h is the Planck constant, and $\Delta\alpha = 1.0\,\text{Å}^3$; thus the rotational period of the N_2 molecule can be obtained by $T_{\mathrm{rot}} = 1/(2Bc) \approx 8.38$ ps. The central wavelength of the pulses is 800 nm and the duration of the pulses is $\tau = 40$ fs.

We first calculate the spectral changes of the probe pulse with input energy of 0.05 mJ depending on the time delay (0.5–20 ps) to only one pump pulse of 0.2 mJ at temperature 25 °C and gas pressure 0.5 bar, and the results are presented in Fig. 1. The spectral blueshift or redshift is observed obviously, and the central wavelength tuning of the probe pulse is different with respect to time delay. Furthermore, with increasing the time delay, the spectral shift exhibits periodic changes and the period is about 8.39 ps, agreeing well with the rotational period of the N_2 molecule T_{rot}. Figure 2 shows the temporal and spectral intensities of probe pulse with (blue solid curves) or without (red dashed curves) considering the effect of molecular alignment, together with the initial probe pulse (green dash-dotted curves), and the same parameters are used as in Fig. 1 but for the probe matching the molecular alignment revival is at time delay 4.20 ps. In Fig. 2(b), it is observed that the spectral profiles for considering the molecular alignment display the blueshift, and the central wavelength shift is ~24 nm; thus the results of wavelength tuning are caused by the influence of molecular alignment based on HCF.

When the pump pulse interacts with the molecular gas, rotational wave packets are created in each molecule, leading to the periodic revivals of molecular alignment. The time-delayed probe pulse experiences molecular phase modulation owing to refractive index variation excited by the molecular alignment revivals, which will generate central wavelength tuning. The time-dependent averaged degree of molecular alignment can be described by $\langle\langle\cos^2\theta\rangle\rangle(t)$, and the refractive

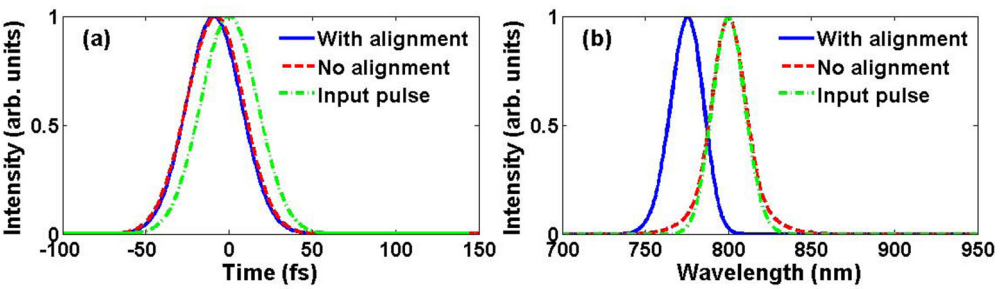

FIG. 2. (Color online) The temporal (a) and spectral (b) profiles of probe pulse, blue solid lines, and red dashed lines, with or without considering the effect of molecular alignment at the same simulation parameters as in Fig. 1 except for time delay 4.20 ps, respectively; green dash-dotted lines represent initial probe pulse.

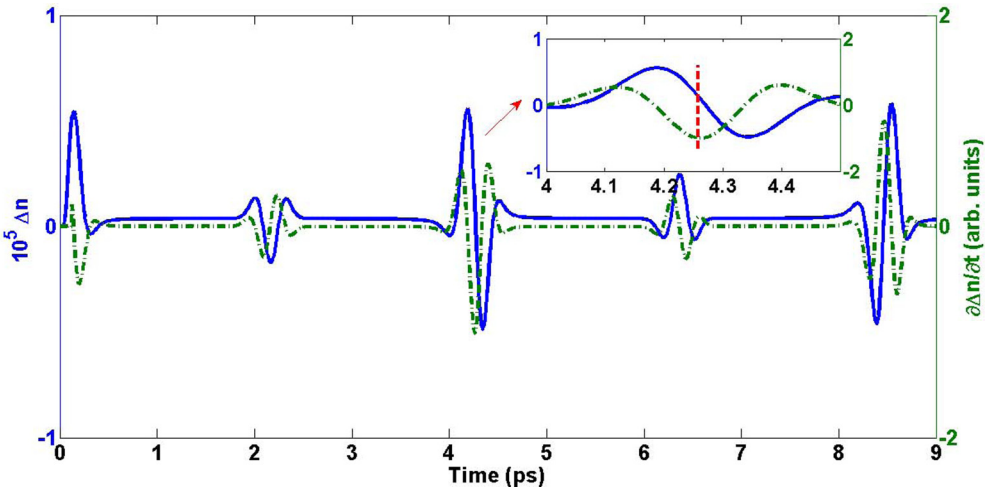

FIG. 3. (Color online) Time evolution of the refractive index change (blue solid lines) and its derivative with respect to time (green dash-dotted lines) induced by a laser pulse with duration 40 fs and energy 0.2 mJ at 25 °C; the optimal time marked in red dashed lines is the negative maximum value of $\partial\Delta n(t)/\partial t$.

index change originated from molecular alignment reads as $\Delta n(t) = 2\pi(\rho_0\Delta\alpha/n_0)[\langle\langle\cos^2\theta\rangle\rangle(t) - 1/3]$; meanwhile, the frequency shift of the probe pulse induced by the effect of molecular alignment maintains such a relationship, $\delta\omega(t) \sim -\partial\Delta n(t)/\partial t$. Figure 3 shows the time-dependent refractive index change $\Delta n(t)$ (blue solid curves) and its derivative $\partial\Delta n(t)/\partial t$ (green dash-dotted curves) created by the pump pulse of energy 0.2 mJ and duration 40 fs at 25 °C. As shown in Fig. 3, the optimal time (4.25 ps) marked in red dashed curves is the negative maximum value of $\partial\Delta n(t)/\partial t$, which means the probe pulse will obtain the maximum blueshift when its temporal peak interacts with the molecular alignment at that moment. The time delay between the pump and probe pulses can be calculated by the optimal time minus the time (0.06 ps) before the temporal peak of the probe pulse is coupled into gas cell, and the result is 4.19 ps in agreement with the case of time delay 4.20 ps in Fig. 1. In conjunction with Figs. 1 and 3, the probe pulse shows a spectral blueshift or redshift as its temporal peak is tuned to the falling or rising edge of the refractive index change (or averaged degree of molecular alignment).

To improve the central wavelength tuning range of the probe pulse, we investigate the influence of pump energy, gas pressure, and temperature in HCF based on the relationship $\delta\omega(t) \sim -\partial\Delta n(t)/\partial t$. Figure 4(a) shows the spectral intensities of the probe pulse by varying pump pulse energy. It clearly suggests the wavelength tuning range is enhanced by increasing the pump energy in the beginning, while it will be

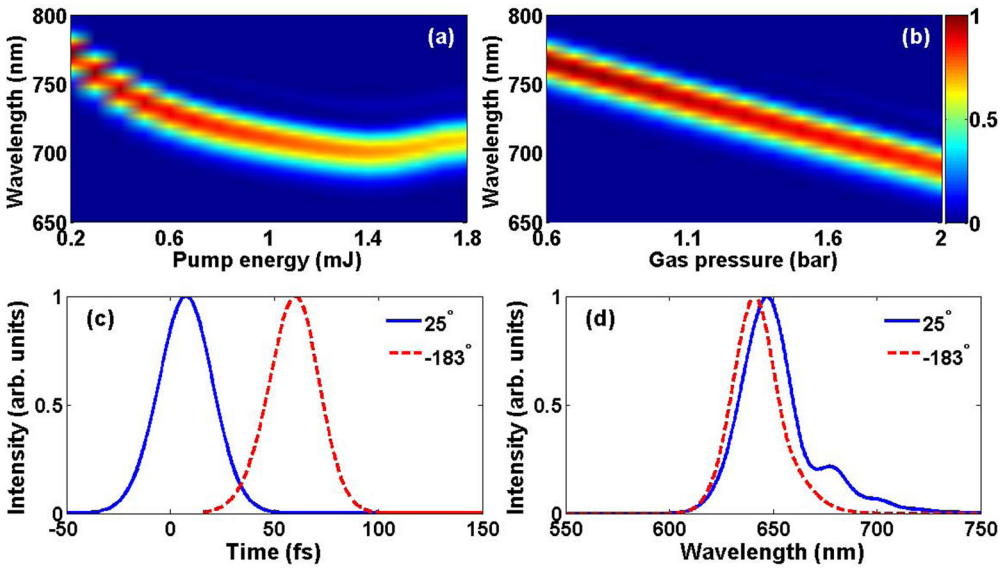

FIG. 4. (Color online) The spectral intensities of output probe pulse for different pump energies (a) from 0.2 mJ to 1.8 mJ and gas pressures (b) from 0.6 to 2.0 bars, respectively; other parameters are the same as in Fig. 2 except for the pump energy for (a) or gas pressure for (b); the temporal (c) and spectral (d) profiles of probe pulse, blue solid lines, and red dashed lines represent the gas temperature 25 °C and −183 °C with pump energy 1.0 mJ, gas pressure 1.0 bar, and time delay 4.20 ps, respectively.

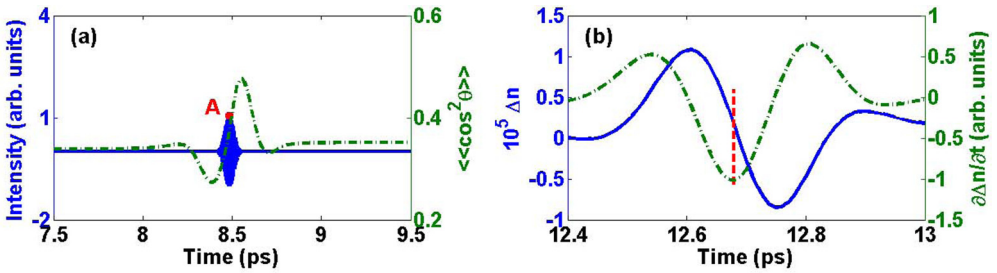

FIG. 5. (Color online) (a) The intensity (blue solid lines) of the second pump pulse and averaged degree (green dash-dotted lines) of molecular alignment by the first pump pulse; the red dot A represents the optimal time delay of the second pump pulse after the first pump pulse. (b) Time evolution of the refractive index change (blue solid lines) and its derivative with respect to time (green dash-dotted lines) induced by double pump pulses with duration 40 fs and energy 0.2 mJ at 25 °C; the red dashed lines represent the optimal delay of probe pulse to the second pump pulse.

suppressed because of the abundant nonlinear effects induced by the intense pump pulse. Figure 4(b) plots the spectral profiles of the probe pulse at various gas pressures in HCF. Similarly, we can see the wavelength shift is improved with increase of the gas pressures and seems like a linear relation; it should be noted that the nonlinear effects are also obvious when the gas pressure is set high enough. Then the suitable pump pulse energy and gas pressure are picked out to increase wavelength tuning range. The temporal and spectral intensities of the probe pulse with pump pulse energy 1.0 mJ, and gas pressure 1.0 bar at time delay 4.20 ps for different gas temperature 25 °C (blue solid curves) and −183 °C (red dashed curves) are shown in Figs. 4(c) and 4(d), respectively. As shown in Fig. 4(c), the centroid of the probe pulse profile shifts more toward the positive side when cooling the molecular gas. When switching off the dispersion terms in the simulations, these delays for different temperatures are of small difference. Considering the dispersion in HCF is small, this shift with temperature can be explained as the combined interaction between linear and nonlinear effects. Note that in Fig. 4(d), a tail exists in the right side of the spectrum of the probe pulse at 25 °C, which suggests the intense pump pulse energy and gas pressure strengthen the nonlinear effects in HCF even though the probe pulse energy of 0.05 mJ is low. However, when the gas temperature is lower, a smooth spectrum is obtained and the wavelength shifts more than ∼159 nm compared with the former case of 25 °C (∼153 nm). That means cooling decreases the nonlinear influence and increases the purity of the molecular coherent state, resulting in a smoother spectrum and wavelength tuning range.

Another method further to improve the value of $\partial\Delta n(t)/\partial t$ is to use double (or even multiple) pump pulses. Figure 5(a) shows the averaged degree (green dash-dotted curves) of molecular alignment before and after the second pump pulse, together with the intensity (blue solid curves) of the second pump pulse with duration 40 fs and energy 0.2 mJ. The time delay of the second pump pulse after the first pump pulse is set at the position of the temporal peak and is marked by the red dot (A). It can be seen that the averaged degree of molecular alignment $\langle\langle\cos^2\theta\rangle\rangle$ is enhanced in Fig. 5(a). The time-dependent refractive index change $\Delta n(t)$ and its derivative $\partial\Delta n(t)/\partial t$ created by the double pump pulses are given in Fig. 5(b); the optimal time delay of the probe pulse to the second pump pulse is marked by red dashed curves. The value of $\partial\Delta n(t)/\partial t$ is obviously increased compared with Fig. 3 induced by a pump pulse.

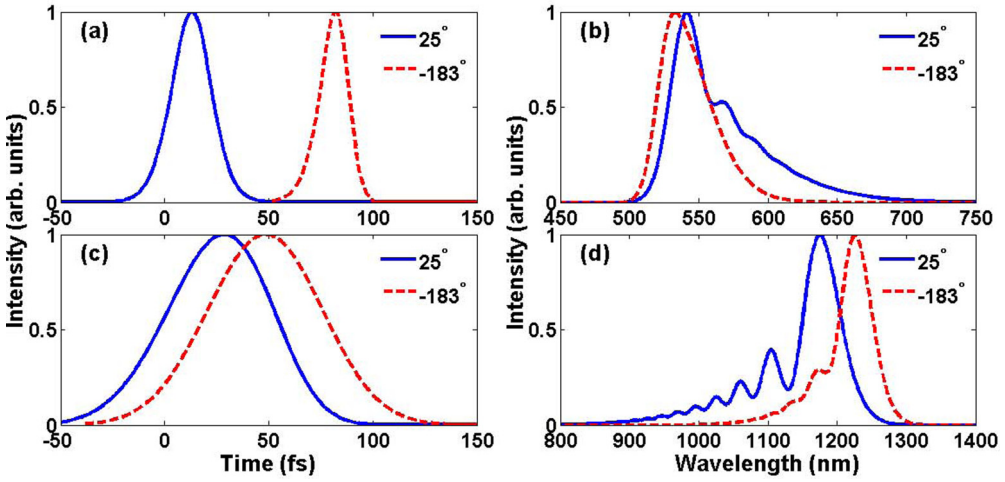

FIG. 6. (Color online) The temporal (a,c) and spectral (b,d) profiles of probe pulse. (a,b) and (c,d) describe the blueshift and redshift of probe pulse with time delay 4.21 and 8.40 ps, respectively. Blue solid lines and red dashed lines represent the gas temperature 25 °C and −183 °C with double pump pulses of energy 1.0 mJ and gas pressure 1.0 bar, respectively.

Based on the previous analysis, there are many ways—such as using an intense pump pulse, increasing the gas pressure, cooling the molecular gas, and using the double pump pulses—to improve the value of $\partial\Delta n(t)/\partial t$ so as to extend the central wavelength tuning range. Figure 6 describes the larger blueshift [Figs. 6(a) and 6(b)] and redshift [Figs. 6(c) and 6(d)] of the probe pulse created by the double pump pulses with even higher energy of 1.0 mJ and gas pressure of 1.0 bar at 25 °C (blue solid curves) and −183 °C (red dashed curves) for different time delays 4.21 and 8.40 ps relative to the second pump pulse, respectively. The blueshifts of probe pulse at 25 °C and −183 °C are ∼259 and ∼267 nm, and are smaller compared with the redshifts ∼375 and ∼426 nm. Therefore, by using intense double pump pulses, we obtain several hundred nanometers wavelength tuning of the probe pulse at different delays.

IV. CONCLUSION

In summary, we have shown numerically the central wavelength tuning of a probe pulse by using ultrafast molecular phase modulation in HCF filled with prealigned nitrogen gas. We demonstrate that the probe pulse experiences a spectral blueshift or redshift depending on whether its temporal peak is tuned to the falling or rising edge of the molecular alignment revival. It is found that using an intense pump pulse energy, increasing gas pressure, cooling gas temperature, and using the double pump pulses can improve the wavelength shift range of the probe pulse. It is also shown that hundreds of nanometers wavelength tuning is achieved by using the double pump pulses with suitable parameters. This method provides us an alternative approach to tune the central wavelength of an ultrashort laser pulse.

ACKNOWLEDGMENTS

This work was partly supported by the National Natural Science Foundation of China (Grants No. 11204328, No. 61221064, No. 61078037, No. 11127901, No. 11134010, and No. 61205208), the National Basic Research Program of China (Grant No. 2011CB808101), and the Natural Science Foundation of Shanghai, China (Grant No. 13ZR1414800).

[1] J. Zhou, J. Peatross, M. M. Murnane, H. C. Kapteyn, and I. P. Christov, Phys. Rev. Lett. **76**, 752 (1996).
[2] P. M. Paul, E. S. Toma, P. Breger, G. Mullot, F. Auge, Ph. Balcou, H. G. Muller, and P. Agostini, Science **292**, 1689 (2001).
[3] X. Feng, S. Gilbertson, H. Mashiko, H. Wang, S. D. Khan, M. Chini, Y. Wu, K. Zhao, and Z. Chang, Phys. Rev. Lett. **103**, 183901 (2009).
[4] I. V. Litvinyuk, K. F. Lee, P. W. Dooley, D. M. Rayner, D. M. Villeneuve, and P. B. Corkum, Phys. Rev. Lett. **90**, 233003 (2003).
[5] T. Suzuki, S. Minemoto, T. Kanai, and H. Sakai, Phys. Rev. Lett. **92**, 133005 (2004).
[6] Y. Liu, X. Liu, Y. Deng, C. Wu, H. Jiang, and Q. Gong, Phys. Rev. Lett. **106**, 073004 (2011).
[7] D. Strickland and G. Mourou, Opt. Commun. **56**, 219 (1985).
[8] D. Wang, Y. Leng, and Z. Huang, J. Opt. Soc. Am. B **31**, 1248 (2014).
[9] G. Cerullo and S. De Silvestri, Rev. Sci. Instrum. **74**, 1 (2003).
[10] A. Dubietis, G. Jonušauskas, and A. Piskarskas, Opt. Commun. **88**, 437 (1992).
[11] I. N. Ross and P. Matousek, J. Opt. Soc. Am. B **19**, 2945 (2002).
[12] L. Bergé, Opt. Express **16**, 21529 (2008).
[13] L. Bergé, J. Rolle, and C. Köhler, Phys. Rev. A **88**, 023816 (2013).
[14] G. Méjean, J. Kasparian, J. Yu, S. Frey, E. Salmon, R. Ackermann, J. P. Wolf, L. Bergé, and S. Skupin, Appl. Phys. B **82**, 341 (2006).
[15] N. Zhavoronkov and G. Korn, Phys. Rev. Lett. **88**, 203901 (2002).
[16] R. A. Bartels, T. C. Weinacht, N. Wagner, M. Baertschy, C. H. Greene, M. M. Murnane, and H. C. Kapteyn, Phys. Rev. Lett. **88**, 013903 (2001).
[17] F. Zhong, H. Jiang, and Q. Gong, J. Opt. Soc. Am. B **27**, 128 (2010).
[18] F. Wang, H. Jiang, and Q. Gong, J. Opt. Soc. Am. B **29**, 232 (2012).
[19] H. Cai, J. Wu, A. Couairon, and H. Zeng, Opt. Lett. **34**, 827 (2009).
[20] P. J. Bustard, B. J. Sussman, and I. A. Walmsley, Phys. Rev. Lett. **104**, 193902 (2010).
[21] M. Li, H. Pan, Y. Tong, C. Chen, Y. Shi, J. Wu, and H. Zeng, Opt. Lett. **36**, 3633 (2011).
[22] F. Zhong, H. Jiang, and Q. Gong, Opt. Express **17**, 1472 (2009).
[23] R. Torres, R. de Nalda, and J. P. Marangos, Phys. Rev. A **72**, 023420 (2005).
[24] S. Zhang, C. Lu, J. Shi, T. Jia, Z. Wang, and Z. Sun, Phys. Rev. A **84**, 013408 (2011).
[25] S. Xu, Y. Yao, C. Lu, J. Ding, T. Jia, S. Zhang, and Z. Sun, Phys. Rev. A **89**, 053420 (2014).
[26] C. Courtois, A. Couairon, B. Cros, J. R. Marques, and G. Matthieussent, Phys. Plasmas **8**, 3445 (2001).
[27] Y. Wang, X. Dai, J. Wu, L. Ding, and H. Zeng, Appl. Phys. Lett. **96**, 031105 (2010).
[28] N. Berti, P. Béjot, J. P. Wolf, and O. Faucher, Phys. Rev. A **90**, 053851 (2014).
[29] L. Bergé, S. Skupin, R. Nuter, J. Kasparian, and J. P. Wolf, Rep. Prog. Phys. **70**, 1633 (2007).
[30] J. Wu, H. Cai, A. Couairon, and H. Zeng, Phys. Rev. A **79**, 063812 (2009).